Michigan State University

National Superconducting Cyclotron Laboratory

MULTI-FRAGMENT PRODUCTION FOR REACTIONS OF $^{112}Sn + ^{112}Sn$ AND $^{124}Sn + ^{124}Sn$ AT E/A = 40 MeV

G.J. KUNDE, S.J. GAFF, C.K. GELBKE, T. GLASMACHER, M.J. HUANG, R.C. LEMMON, W.G. LYNCH, L. MANDUCI, L. MARTIN, M.B. TSANG, W.A. FRIEDMAN, J. DEMPSEY, R.J. CHARITY, L.G. SOBOTKA, D.K. AGNIHOTRI, B. DJERROUD, W.U. SCHRÖDER, W. SKULSKI, J. TÖKE, and K. WYROZEBSKI

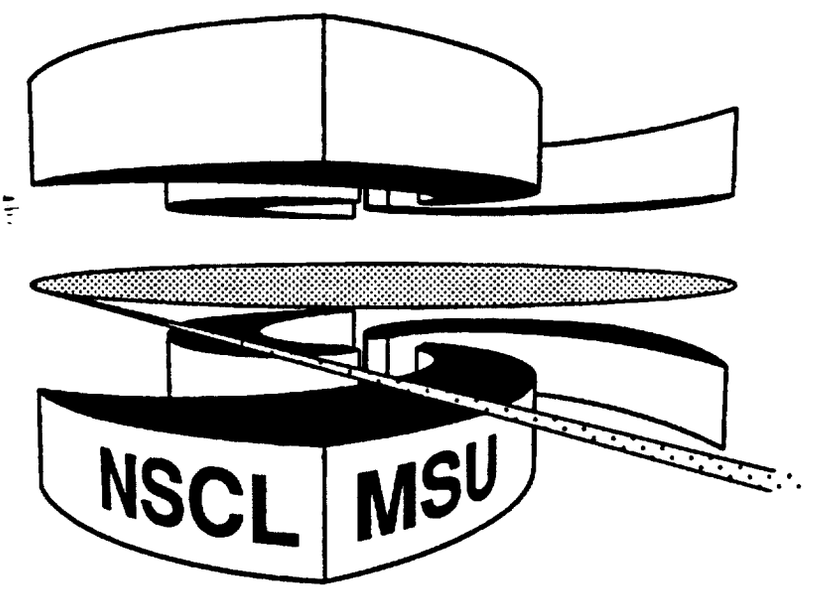

MSUCL-1043 SEPTEMBER 1996

Multi-fragment production for reactions of ^{112}Sn + ^{112}Sn and ^{124}Sn + ^{124}Sn at E/A = 40 MeV

G.J. Kunde, S.J. Gaff, C.K. Gelbke, T. Glasmacher, M.J. Huang, R. Lemmon,

W.G. Lynch, L. Manduci, L. Martin, M.B. Tsang

Department of Physics and Astronomy and National Superconducting Cyclotron Laboratory, Michigan State University, East Lansing, MI 48824, USA

W.A. Friedman

Department of Physics, University of Wisconsin, Madison, WI 53706, USA

J. Dempsey, R.J. Charity, L.G. Sobotka

Department of Chemistry, Washington University, St. Louis, MO 63130, USA

D.K. Agnihotri, B. Djerroud, W.U. Schröder, W. Skulski, J. Tõke, K. Wyrozebski

Department of Chemistry and Nuclear Structure Research Laboratory, University of Rochester, Rochester, NY 14627, USA

Abstract

Multiplicities of intermediate-mass fragments (IMFs), neutrons, and charged particles were measured for ^{112}Sn + ^{112}Sn and ^{124}Sn + ^{124}Sn at E/A = 40 MeV. Significantly different scalings of the mean IMF-multiplicities with neutron and charged-particle multiplicities are observed for the two reactions. These differences can be qualitatively understood in terms of fragment emission from an expanding evaporating source for which the initial rates of cooling by neutron and light-charged-particle emission depend on the neutron and proton numbers of the source according to statistical expectations.

Hot nuclear systems formed in intermediate energy nucleus-nucleus collisions are known [1-8] to decay by copious production of intermediate mass fragments (IMF's) characterized by $3 \leq Z_{IMF} \leq 20$. In examining reactions of Xe on various targets covering a wide range of masses, a near-universal correlation has previously been observed between the average number of emitted IMFs, $< N_{IMF} >$, and the charged particle multiplicity, NC [7]. In reactions, using reversed kinematics, with Au beams on a variety of targets, a similar universal correlation (independent of target mass) was also observed between $< N_{IMF} >$ and the total charge contained in fragments having two or more charges, which were observed near the projectile rapidity [8-10]. The universality seen in these instances was interpreted as due to a decay mechanism, independent of the production of the decaying system.

Only a few studies have addressed the influence of the neutron number of the projectile or target. Observables studied so far were isotopic yields of fragments [11-13] and isobaric ratios [14]. In this letter we investigate the influence of the neutron number in the target and projectile on the correlation of $< N_{IMF} >$ with the multiplicities of the yields of different types of particles: charged particles (N_C), neutrons (N_N), and light-charged particles with $Z \leq 2$ (N_{LC}) [15]. The measurement involves reactions with two projectile-target combinations of fixed proton number (to keep the influence of the Coulomb force constant), but very different neutron numbers. Specifically, we studied collisions of $^{112}Sn + ^{112}Sn$ and $^{124}Sn + ^{124}Sn$ at E/A = 40 MeV by means of an experimental setup which provided simultaneous $4 - \pi$ coverage for neutrons and charged particles. In contrast to the previously cited universal scaling, we observe significant differences between the reactions in the correlations of $< N_{IMF} >$ with N_C, N_N, and N_{LC}. These differences can be qualitatively understood in terms of the expanding evaporating source model [16] which has previously been shown to explain the large number of fragments observed in central heavy ion collisions [5,6] as well as the low observed temperatures at which the fragments were produced [16,17].

The experiment was performed at the National Superconducting Cyclotron Laboratory at Michigan State University. Two symmetric reactions, $^{112}Sn + ^{112}Sn$ and $^{124}Sn + ^{124}Sn$, were studied at a beam energy of E/A = 40 MeV. The areal density of the targets was $5 mg/cm^2$.

For each event, the associated neutron multiplicity was measured with the SuperBall neutron multiplicity meter [18] and charged particles were detected in 280 plastic scintillator - CsI(Tl) phoswich detectors of the Miniball/Miniwall array [19]. The charged particle arrays provided isotopic resolution for H and He nuclei and elemental resolution for heavier fragments with approximate energy thresholds of $E_{th}/A \approx 2.2$ MeV (4.5 MeV) for Z=3 (Z=10) particles detected in the Miniwall at $5.4° \leq \Theta_{lab} \leq 25°$ and $E_{th}/A \approx 1.5$ MeV (2.5 MeV) for Z=3 (Z=10) particles detected in the Miniball at $25° \leq \Theta_{lab} \leq 160°$ respectively. The event trigger required the detection of at least two charged particles.

Figure 1 shows the observed average neutron multiplicities, $< N_N >$, as a function of charged-particle multiplicity, N_C. Since heavy nuclei of moderate excitation energy decay primarily by neutron emission, the event trigger largely suppresses very peripheral collisions characterized by low neutron multiplicities. For a given value of N_C, larger neutron multiplicities are observed for ^{124}Sn + ^{124}Sn than for ^{112}Sn + ^{112}Sn. This dependence of neutron multiplicity on the neutron-to-proton ratio of the emitting system is consistent with simple expectations.

Figure 2 shows the average number of detected intermediate mass fragments ($< N_{IMF} >$: $Z \geq 3$) as a function of N_C (points, left panel), N_{LC} (curves, left panel), and N_N (points, right panel) for the two reactions studied. Distinct differences are observed which are incompatible with a universal scaling of $< N_{IMF} >$ with N_C, N_{LC}, or N_N. Relative to the respective curves for ^{112}Sn + ^{112}Sn, the $< N_{IMF} >$ versus N_C and N_{LC} curves for ^{124}Sn + ^{124}Sn are shifted to lower values of N_C and N_{LC}, while the $< N_{IMF} >$ versus N_N curve is shifted to higher values of N_N. At any given value of N_C or N_{LC}, $< N_{IMF} >$ is larger for ^{124}Sn + ^{124}Sn than for ^{112}Sn + ^{112}Sn. The same is true for very high values of N_N, where the $< N_{IMF} >$ versus N_N curves have leveled off, but in the region where $< N_{IMF} >$ grows monotonically with increasing N_N, the fragment multiplicity at a given value of N_N is larger for ^{112}Sn + ^{112}Sn than for ^{124}Sn + ^{124}Sn collisions. Roughly consistent with the larger mass of the ^{124}Sn + ^{124}Sn system, the maximum values of $< N_{IMF} >$ are about 10% larger for ^{124}Sn + ^{124}Sn than for ^{112}Sn + ^{112}Sn. Rather surprisingly, the maximum $< N_{IMF} >$-values extracted as a function of N_C

are about 50% larger than those extracted as a function of N_N; those extracted as a function of N_{LC} lie in between.

A detailed understanding of the reaction requires calculations capable of predicting the dynamics of the collision as a function of impact parameter and time and capable of treating fast non-equilibrium emissions, the statistical decay of excited projectile and target residues, and the disintegration of the "neck" [20] temporarily formed in between. Such calculations are beyond the scope of the present work. However, the qualitative trends observed in Fig. 2 are predicted by statistical calculations and are thus largely driven by phase space. To demonstrate this, we use the expanding evaporating source (EES) model of ref. [16] which has been successful in explaining a number of features observed in multifragment emission processes [5,6,16,17]. Since correlations between $< N_{IMF} >$ and N_C depend only weakly on the total mass of the assumed source [5,7], we restrict our schematic calculations to the idealized case of a source made up of the total mass and charge of projectile and target (labeled as $^{224}_{100}$X and $^{248}_{100}$X). Thus, our calculations are best suited for collisions where the overlap of projectile and target is large. (We did verify, however, that the qualitative differences observed for the two systems are also predicted for the other extreme, namely the decay of a projectile and a target-like source – which is more realistic for peripheral collisions.) For simplicity, we assumed a flat distribution of initial temperatures covering an interval of excitation energies per nucleon of 1.3 MeV $\leq E^*/A \leq$ 10 MeV. The upper limit corresponds to the limiting case of complete fusion; the lower limit is arbitrary and of little interest. Since we are primarily interested in providing an understanding of the qualitative differences observed for the two systems, we refrain from filtering the calculations by the acceptance of the experimental apparatus [21].

Figure 3 shows multiplicity correlations calculated for ^{112}Sn + ^{112}Sn and ^{124}Sn + ^{124}Sn. Both the direction and the relative magnitude of the shift between the various multiplicity correlations noted in Fig. 2 are approximately reproduced. The calculations also reproduce the qualitative differences between the maximum values of $< N_{IMF} >$ observed at large N_C, N_{LC}, and N_N.

To illustrate similarities and differences predicted by the model for the decay of the two systems, we show in Fig. 4 the predicted time-dependence of source temperatures (dotted curves, right hand scale) and emission rates of neutrons, light charged particles, and IMFs (dashed, solid, and dot-dashed curves, respectively, left hand scale) assuming a single initial excitation energy per nucleon of $E^*/A = 10$ MeV. Initially, the two sources cool by expansion and light particle emission with very minor differences in their cooling rates. When the sources reach their minimum density (at T $\approx$ 5-6 MeV), they are predicted to decay by copious IMF production. In the model, the system resides for a relatively long time ($\approx$ 100 fm/c) in this low-temprature, low-density configuration (note the logarithmic time scale), and nearly all fragments are emitted during this time interval. After this stage the model sources have lost approximately 1/3 of their original mass and their N/Z ratios have changed from 1.48 (1.24) to approximately 1.45 (1.30) for the neutron rich (neutron poor) systems. A modest subsequent rise in temperature is predicted when the sources contract back to near-normal nuclear density, but subsequent particle emission is less important. The model predicts very different neutron and light-charged-particle emission rates for the two systems, but similar IMF production rates.

Figure 5 shows model predictions of the average initial excitation energy per nucleon, $< E^*/A >$, selected by sharp cuts on N_C, N_{LC} or N_N. Over a significant range of multiplicities, $< E^*/A >$ is proportional to N_C, N_{LC} and N_N. (The flat regions at low and high multiplicities are associated with the sharp edges of the assumed flat initial temperature distribution.) A cut on N_C or N_{LC} selects a higher value of $< E^*/A >$ (and thus a higher value of $< N_{IMF} >$) for the neutron-rich system, but a cut on N_N selects a lower value. The relative difference in excitation energy selection is more pronounced for cuts on N_N than for cuts on N_C or N_{LC}. The offset between the $< N_{IMF} >$ versus N_C, N_{LC} or N_N curves in Fig. 2 can thus be understood as due to the fact that specific cuts on N_C, N_{LC} or N_N select different initial conditions for the two systems.

Maximum $< N_{IMF} >$ values extracted from $< N_{IMF} >$ versus N_C, N_{LC} and N_N correlations are surprisingly different, see Fig. 2. Within the EES model, these difference arise

from two effects. First, the intrinsic resolution of neutron and charged particle multiplicity filters is different. For example, sharp cuts in N_C, N_{LC} and N_N, chosen to select the same average excitation energy per nucleon, $< E^*/A > = 7$ MeV, for the $^{224}_{100}X$ ($^{248}_{100}X$) system, filter out E^*/A - distributions of variances $\sigma^2(E^*/A) \approx 0.9$, 1.32, and 1.82 MeV^2 (0.9, 1.36, 1.64 MeV^2), respectively; i.e., the resolution is predicted to be best for cuts on N_C. Second, in the extreme tails of the N_C, N_{LC}, and N_N distributions, auto-correlations due to energy conservation become apparent. If, for example, all reactions had a single initial excitation energy, the selection of very high neutron or light-charged-particle multiplicity events would produce a sample of reduced IMF multiplicity, i.e. N_N and N_{IMF} (and also N_{LC} and N_{IMF}) are anti-correlated. The opposite is true for N_C and N_{IMF}, because IMFs are included in the definition of N_C [15]. These auto-correlations arise in our model calculations – which predict that they become significant in the extreme tails of the multiplicity distributions. For example, calculations at a fixed initial excitation energy per nucleon of $E^*/A = 9$ MeV predict a change of $\Delta < N_{IMF} > \approx +1(-1)$ when the selecting gate on N_C (N_N) is increased by ΔN_C (ΔN_N) ≈ 10 from its average value.

The effects of these auto-correlations can be studied in the calculations by comparing the average yields calculated at a fixed temperature with the yields which reflect event-to-event fluctuations. As an example we consider calculations for $^{224}_{100}X$. For the highest initial excitation energy used in determining the yields, $E^*/A = 10$ MeV, the average predicted multiplicities are: $\overline{N_{IMF}} = 5.2$, $\overline{N_C} = 41.5$, $\overline{N_{LC}} = 36.2$, and $\overline{N_N} = 28.9$ [22]. The point ($\overline{N_C}$, $\overline{N_{IMF}}$) lies close to the calculated $< N_{IMF} >$ versus N_C curve in Fig. 3, but values of $< N_{IMF} >$ larger than $\overline{N_{IMF}}$ are obtained for $N_C > \overline{N_C}$ due to the positive correlation between N_{IMF} and N_C explained above. In contrast, the maxima of the $< N_{IMF} >$ versus N_{LC} (N_N) curves are smaller than $\overline{N_{IMF}}$, and there are clear signs of an anti-correlation between N_{IMF} and N_{LC} (N_N) in Fig. 3 when N_{LC} (N_N) is significantly larger than $\overline{N_{LC}}$ ($\overline{N_N}$).

The relative magnitudes of resolution and auto-correlation effects in the tails of the multiplicity distributions depend on the assumed distribution of initial excitation energies

and on contributions of prompt particles, and can thus not be disentangled in a model-independent way.

In summary, large differences in the correlations of average IMF multiplicities with neutron, charged-particle, and light-charged-particle multiplicities were observed for ^{112}Sn + ^{112}Sn and ^{124}Sn + ^{124}Sn reactions. These differences can be understood by statistical calculations for an ensemble of expanding evaporating sources representing a broad range of initial temperatures. In the calculations, the observed effects are due to different cooling rates from neutron and light-charged-particle emission, differences in resolution of reaction filters based upon neutron and charged particle multiplicity measurements, and auto-correlations between various emission types at high multiplicities.

This work was supported by the National Science Foundation under Grants No. PHY-9214992, PHY-9314131, and PHY-95-28844. G.J.K. acknowledges support of the Alexander-von-Humboldt Foundation.

References

1. D.H.E. Gross, Rep. Progr. Phys. 53, 605(1990).

2. L. G. Moretto and G. J. Wozniak, Ann. Rev. Nucl. Part. Sci. 43, 379 (1993) and references quoted therein.

3. J.P. Bondorf, A.S. Botvina, A.S. Iljinov, I.N. Mishustin and K. Sneppen, Phys. Rep. 257, 133 (1995).

4. C.A. Ogilvie et al., Phys. Rev. Lett. 67, 1214 (1991).

5. D.R. Bowman et al., Phys. Rev. Lett. 67, 1527 (1991).

6. R.T. de Souza et al., Phys. Lett. B268, 6 (1991).

7. D.R. Bowman et al., Phys. Rev. C46, 1834 (1992).

8. P. Kreutz et al., Nucl. Phys. A556, 672 (1993).

9. J. Pochodzalla et al., Nucl. Phys. A583, 553c (1995).

10. W. Trautmann et al., to be published.

11. J. Brzychczyk et al., Phys. Rev. C47, 1553 (1993).

12. S.J. Yennello et al., Phys. Lett. 321B, 15 (1994).

13. R. Wada et al., Phys. Rev. Lett. 58, 1829 (1987).

14. Yu. Murin et al., Phys. Rev. C51, 2794 (1995).

15. In our definition, $N_{\rm C} = N_{\rm LC} + N_{\rm IMF} + N_{\rm NID}$, where $N_{\rm LC}$, $N_{\rm IMF}$, and $N_{\rm NID}$ denote the multiplicities of light-charged-particles, of intermediate mass fragments, and of non-identified charged particles with $Z \geq 3$, respectively.

16. W.A. Friedman, Phys. Rev. Lett. 60 (1988) 2125; and Phys. Rev. C42 (1990) 667.

17. C. Schwarz et al., Phys. Rev. C48, 676 (1993) and refs. given therein.

18. W.U. Schröder, University of Rochester Report DOE/ER/79048-1, 1995, unpublished.

19. R.T. de Souza et al., Nucl. Instr. and Meth. A295, 109 (1990); M.B. Tsang et al., Phys. Rev. Lett. 71 (1993) 1502.

20. C.P. Montoya et al., Phys. Rev. Lett. 73, 3070 (1994).

21. Details of the kinetic energy spectra depend on the reaction dynamics, i.e. on the number of emitting sources and their velocities; thus the effects of experimental acceptance cannot be assessed reliably for the schematic EES model.

22. We use a different notation for the average values at fixed $E^*/A = 10$ MeV to distinguish them from the average IMF multiplicities, $< N_{\rm IMF} >$, extracted from cuts on the fluctuating quantities $N_{\rm C}$, $N_{\rm LC}$, or $N_{\rm N}$.

Figure Captions

Fig. 1: Average neutron multiplicities, $< N_N >$, as a function of charged-particle multiplicity, N_C, for $^{112}Sn + ^{112}Sn$ and $^{124}Sn + ^{124}Sn$ collisions at E/A = 40 MeV.

Fig. 2: Average fragment multiplicities, $< N_{IMF} >$, as a function of charged-particle and light-charged-particle multiplicities (N_C and N_{LC}, left panel) and neutron multiplicities (N_N, right panel) for $^{112}Sn + ^{112}Sn$ (open points and dashed curves) and $^{124}Sn + ^{124}Sn$ (solid points and solid curves) collisions at E/A = 40 MeV.

Fig. 3: Average fragment multiplicities, $< N_{IMF} >$, predicted by the EES model as a function of charged-particle and light-charged-particle multiplicities (N_C and N_{LC}, left panel) and neutron multiplicities (N_N, right panel) for $^{112}Sn + ^{112}Sn$ and $^{124}Sn + ^{124}Sn$. Details of the calculations are discussed in the text.

Fig. 4: Particle emission rates and cooling curves predicted by the EES model for initial source temperatures of 13 MeV. Top and bottom panels show results for $^{112}Sn + ^{112}Sn$ and $^{124}Sn + ^{124}Sn$, respectively.

Fig. 5: Average source excitation energy per nucleon, $< E^*/A >$, selected by sharp cuts on N_C and N_{LC} (circles points and lines, left panel) and N_N (points, right panel) as predicted by EES calculations for $^{112}Sn + ^{112}Sn$ and $^{124}Sn + ^{124}Sn$.

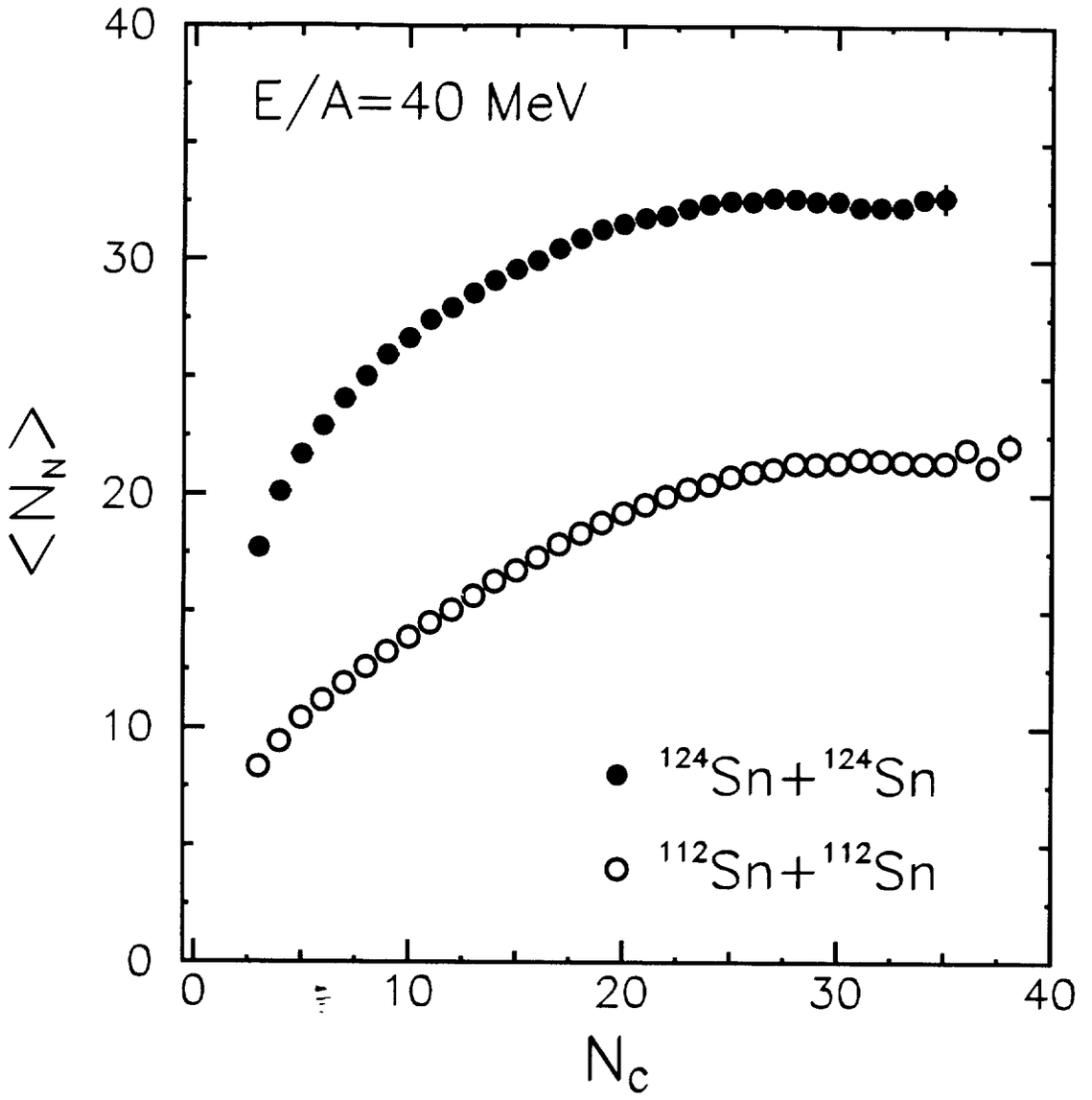
E/A=40 MeV
^{124}Sn+^{124}Sn
^{112}Sn+^{112}Sn
$\langle N_n \rangle$
N_c
0
10
20
30
40

Fig. 1

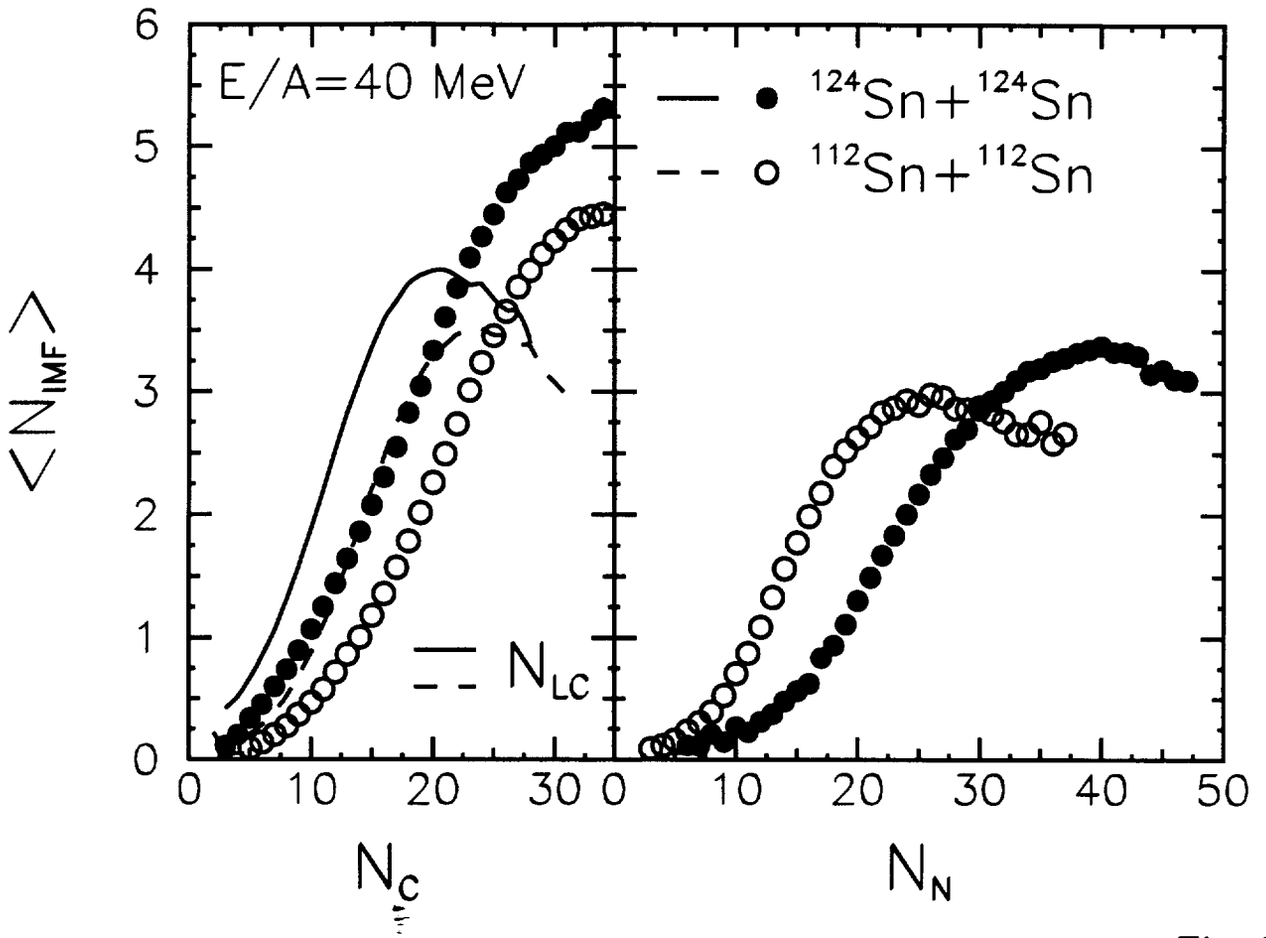
E/A=40 MeV
^{124}Sn+^{124}Sn
^{112}Sn+^{112}Sn
N_{LC}
$\langle N_{IMF} \rangle$
N_C
N_N
0
1
2
3
4
5
6
0
10
20
30
40
50

Fig. 2

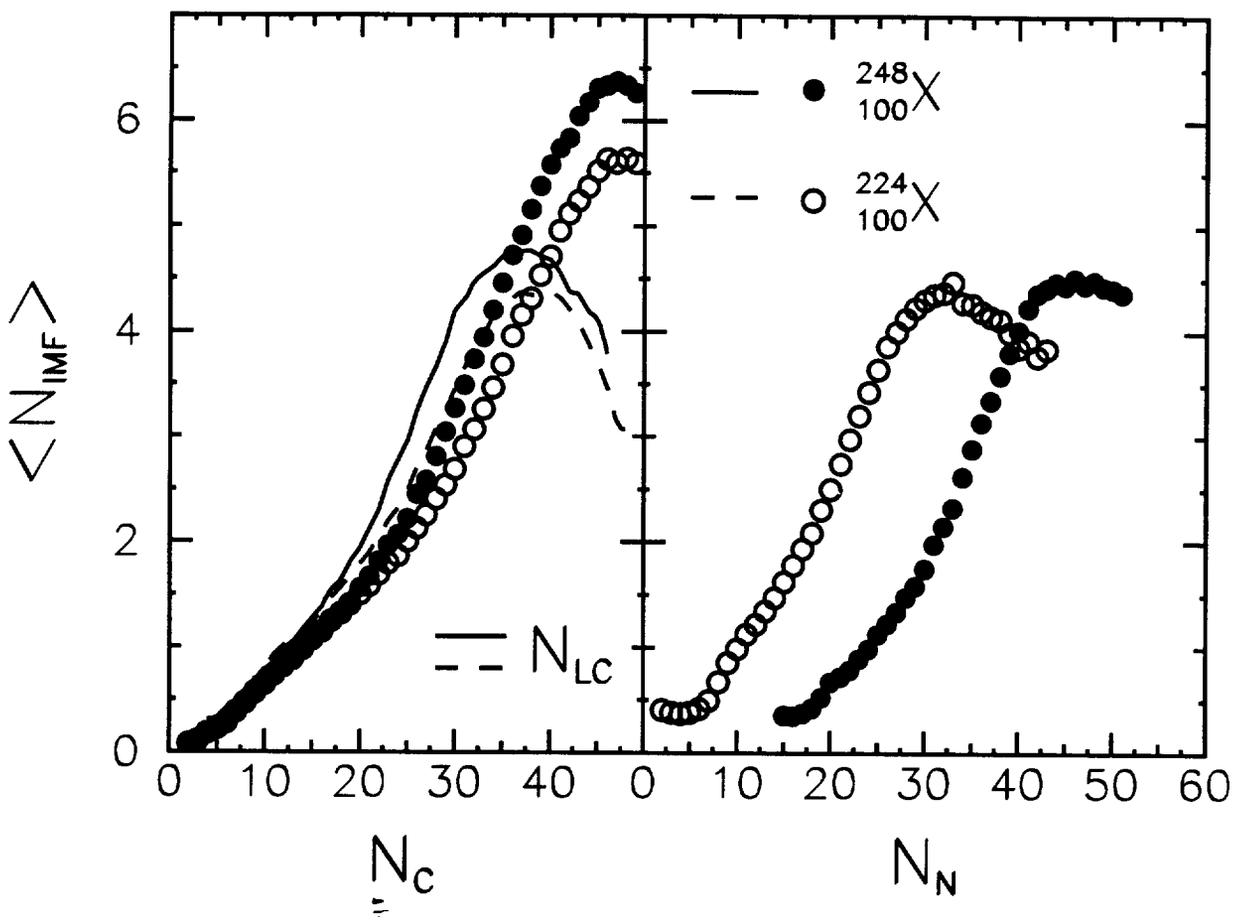
$\langle N_{IMF} \rangle$
6
4
2
0
0 10 20 30 40
N_C
N_{LC}
$^{248}_{100}X$
$^{224}_{100}X$
0 10 20 30 40 50 60
N_N

Fig. 3

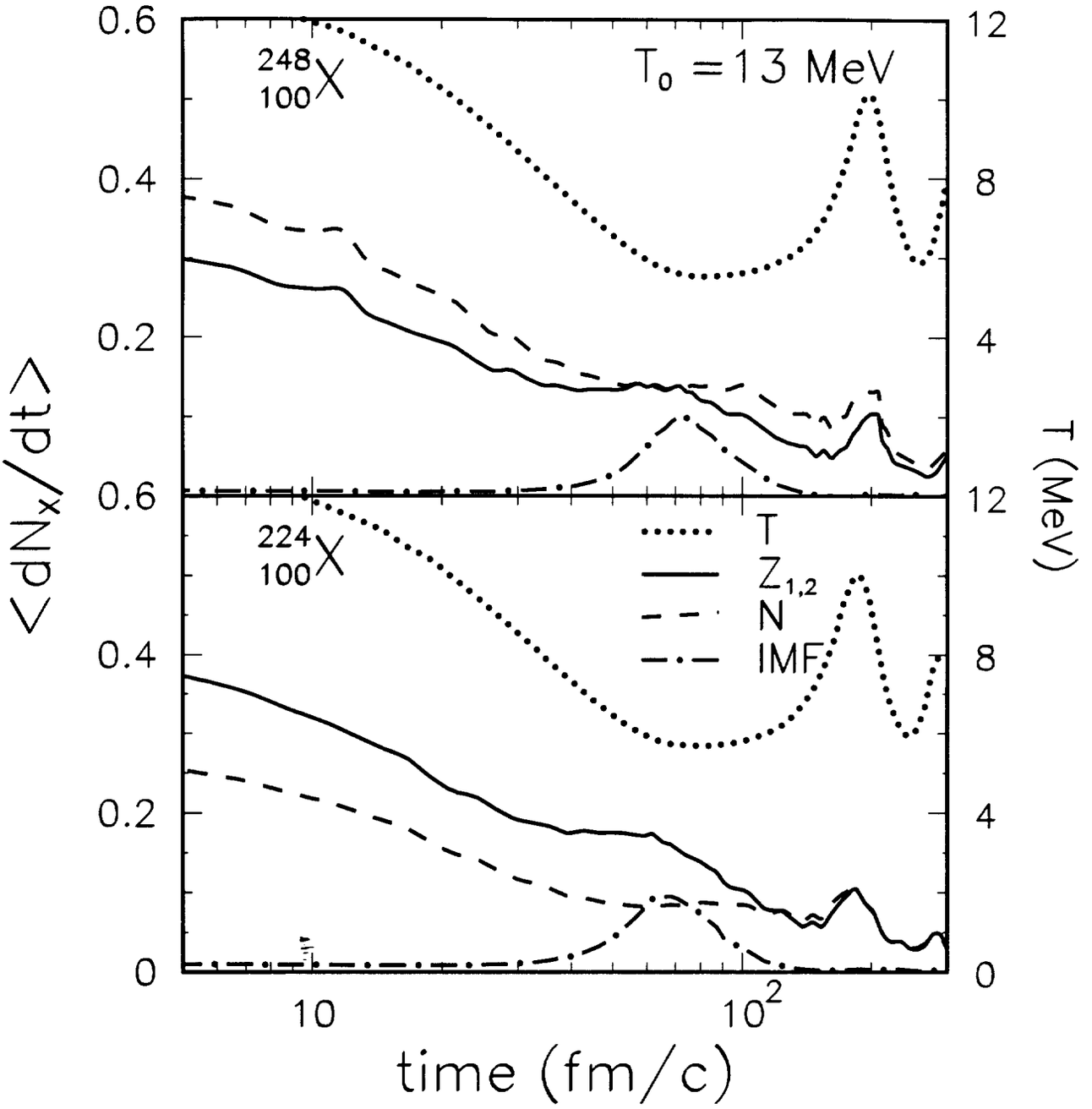
0.6
0.4
0.2
0
248
100X
$T_0 = 13$ MeV
224
100X
T
$Z_{1,2}$
N
IMF
12
8
4
0
10
10^2
time (fm/c)
$<dN_x/dt>$
T (MeV)

Fig. 4

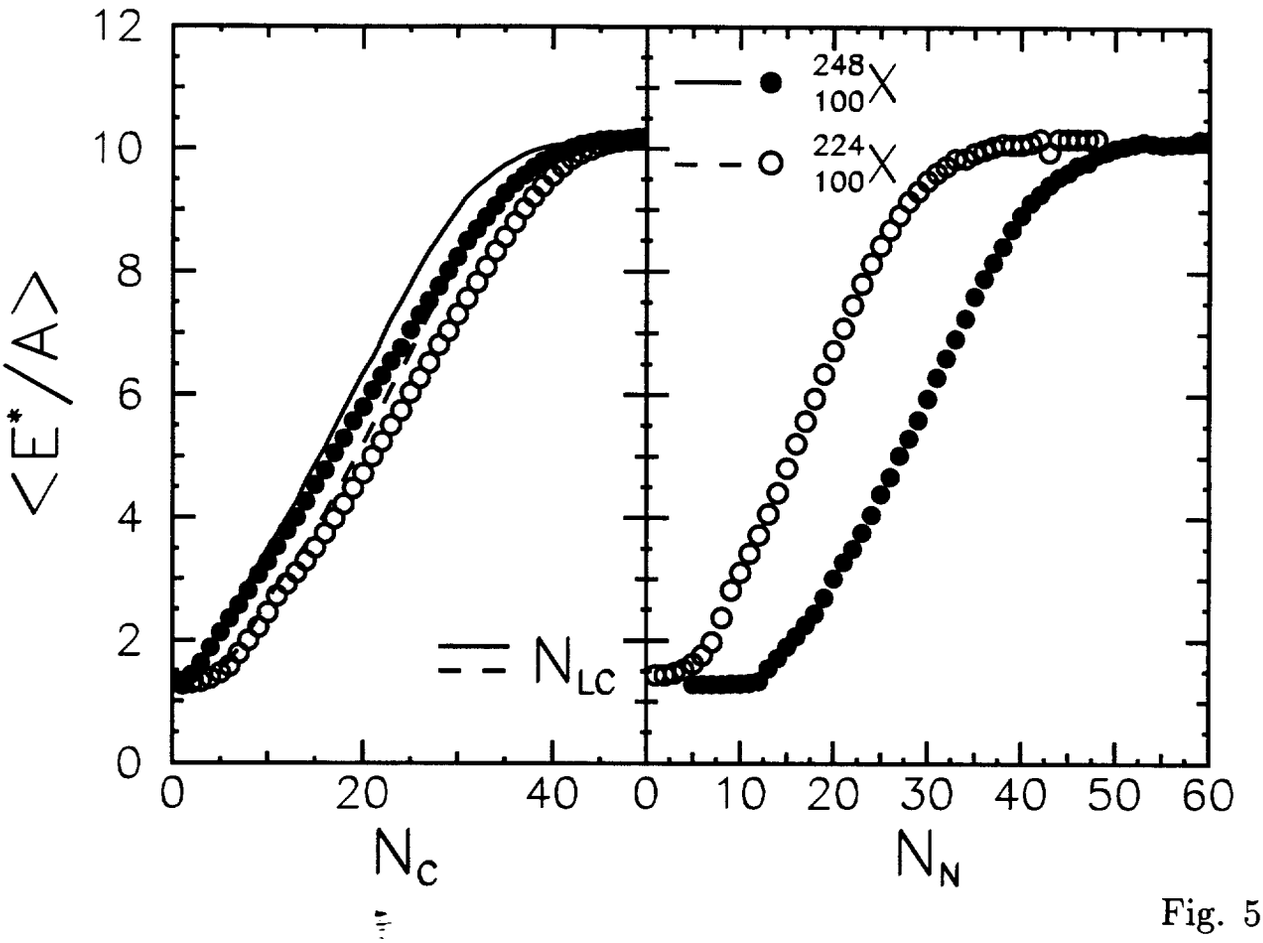
12
10
8
6
4
2
0
$\langle E^*/A \rangle$
0
20
40
N_C
N_{LC}
248 100X
224 100X
0
10
20
30
40
50
60
N_N

Fig. 5